Experimental characterization of interlaminar fracture toughness of composite laminates assembled with three different carbon fiber lamina

Domenico Gentile
University of Cassino and Southern Lazio, Cassino (FR), Italy
gentile@unicas.it

ABSTRACT. In the present work, the fracture resistance of a carbon fiber composite under mode I and mode II loading have been experimentally determined. For the mode I and II, the energy release rate G has been determinate for each material. In some cases, only a single estimation of G was possible due to problems in the propagation such as extensive fiber bridging and loss of planarity of the running crack. The experimental results relative to DCB tests have been analyzed in order to derive statistical trends. Only the samples for which more than three crack advance data points have been collected are considered in the analysis. The G values are those obtained with the compliance calibration method (CC). For ENF test, determination of critical GII, in addition to the value calculated with the relationship given in the prescription EN6034, other two values, the non linear and visual non linear, are also given. The crack propagation resulted to be unstable for all specimens tested and only a single value of GII could be determined.

KEYWORDS. Carbon fiber; Delamination; ENF; DCB.

Citation: Gentile, D., Experimental characterization of interlaminar fracture toughness of composite laminates assembled with three different carbon fiber lamina, Frattura ed Integrità Strutturale, 43 (2018) 155-170.

Received: 21.09.2017
Accepted: 05.11.2017
Published: 01.01.2018

INTRODUCTION

Composites based on carbon fiber are widely used in the field of automobiles, aircrafts, and spacecrafts. These materials, it is well known, give some advantages in terms of specific modulus and specific strength comparing with the traditional metals. Another important point is the possibility to design structures that are more efficient by changing mechanical properties with variable reinforcing methods.
For this reason, it is very important to assure the reliability of the components against interlaminar fracture, because the weakest fracture mode depends on the interlaminar crack.
The fracture behavior of unidirectional, quasi-isotropic, and woven reinforced laminates carbon fiber composites has been mainly investigated, [1-12].
Interlaminar flaws, or delaminations, can be generated in the composite material during the production process, as a consequence of the contamination of the prepeg which may result in regions with poor adhesion between plies, or they can

start from regions of the composite with an elevated void volume fraction. Alternatively, these flaws can be initiated by post-production handling or by the action of the external load during the service life. Damage tolerance design approach to composite structures requires to establish the critical conditions, in terms of maximum allowable flow size and design loads, which may be sustained without the risk of unstable flaw propagation or the drop of the nominal design material resistance below acceptable limits.

From a conceptual point of view, interlaminar flaws are bidimensional discontinuities that can be treated as cracks with a non-straight front, in general. Conditions for stable or unstable crack propagation may be reached during the application of thermo-mechanical loads when the intensity of the stress field at the crack tip exceeds a critical value typical for the material under investigation. Due to the similarity to planar cracks, delaminations can be correctly analyzed with fracture mechanics tools. The appropriate parameter that characterizes composite laminate resistance to the propagation of an interlaminar flaw is the unitary strain energy release rate, G.

Moreover, interlaminar cracks might develop in many of the load cases that are likely to develop under normal use of aerostructures, e.g. at concentrated loads at joints and due to un-avoidable impact loads. These cracks are very difficult to detect and their presence may severely reduce the load carrying capacity of the component. Thus, modelling of the interlaminar behavior is crucial for safe design of an advanced structural component; especially when initiation of cracks is studied, [6]. This is means that in order to develop a robust model to predict components behavior it is very important to characterize composite laminate resistance to the propagation.

Experimentally Double Cantilever Beam (DCB) and End Notched Flexure (ENF) testing mainly measured the fracture toughness for Mode I and Mode II.

In the present work, the fracture resistance of carbon fiber based laminates under mode I and mode II loading have been experimentally determined. Mixed mode configuration has not been considered at this time.

At present, experimental testing and the procedure for the determination of fracture resistance in composite laminates is coded in the international standards such as ASTM only for unidirectional laminates [0]n with propagating delamination along the fiber direction. In multidirectional laminates, delamination crack may branch through the oriented plies invalidating the fracture mechanics assumption of planar propagation. In addition, secondary effects, such as edge effects, crack tip oscillation, etc., which may strongly affect the estimation of G, are very difficult to be avoided, [7, 8]. As far as concern composite laminates, the procedure for the determination of the laminate fracture resistance under mode I and mixed mode I+II loading conditions are coded in the ASTM D-5528-01 and ASTM D-6671-01, respectively. The test procedure for the determination of G under mode II loading condition followed in the present work, is available in the AECMA book of standards (prEN 6034), [9].

Preliminary considerations and fundamental relationships for laminate fracture resistance under mode I

Laminate fracture resistance under mode I loading configuration can be easily determined on double cantilever beam (DCB) specimen geometry. The reference geometry for the specimen is given in Fig. 1 together with the definition of the fundamental dimensions.

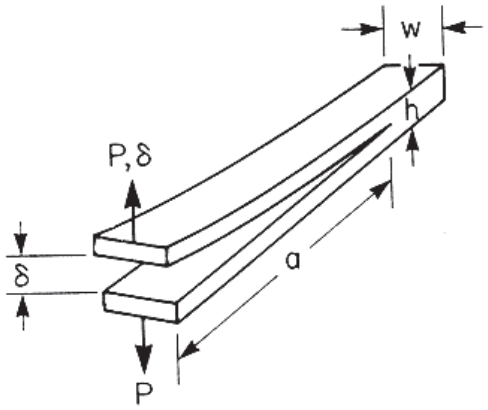

Figure 1: DCB geometry definition

Even though experimental data reduction is not based on the classical beam theory, as initially proposed by Wilkins et al., [1], the simplicity of the theory allows to derive some of the fundamental relationships for this geometry.

In this approximation, the geometry compliance is given by:

$$C = \frac{\delta}{P} = \frac{2a^3}{3E_{11}I} \tag{1}$$

while the strain energy release rate for unitary surface crack advance is given by:

$$G_I = \frac{P^2 a^2}{wE_{11}I} \tag{2}$$

The condition for stable crack growth is given by:

$$\frac{\partial G_I}{\partial a} \le 0 \tag{3}$$

That for the DCB configuration is verified only for the imposed displacement conditions:

$$\left.\frac{\partial G_I}{\partial a}\right|_{\delta=const} = -\frac{4\delta^2 a}{C^2 wE_{11}I} \tag{4}$$

For the imposed load conditions, the DCB configuration is intrinsically unstable since the derivative is always greater than zero:

$$\frac{\partial G_I}{\partial a} = \frac{2P^2 a}{wE_{11}I} > 0 \tag{5}$$

The relation given in Eqn. (1) also requires the value of the elastic traction modulus along the fiber direction. This can be a considerable source of error in the estimation of G_I due to the uncertainties and accuracy of the Young modulus. For instance, an accuracy of ± 10 GPa results in an uncertainty of ± 7% in the estimation of the value of G. In addition to this, the error due to the fact that the shear compliance is neglected in the beam theory have also to be considered. Alternatively, G_I can be expressed in term of quantities directly measurable in the DCB traction test such as the displacement along the load line and the applied load. According to this the resulting expression for G is given by

$$G_I = \frac{nP\delta}{2ba} \tag{6}$$

Eqn. (6) is usually indicated as Compliance Calibration Method (CCM) since the coefficient n corrects the beam theory approximated solution. In the case of perfect load fixtures and Modified Beam Theory (MBT), the coefficient n is equal to 3:

$$G_I = \frac{3P\delta}{2ba} \tag{7}$$

The values obtained with Eqn. (7) overestimate the effective G values and can be taken as upper bound limit. The effective n value can be obtained as linear regression of the compliance measurements as a function of the crack advance on a double Ln plane as also described in the ASTM E-5528 prescription. This methodology requires a number of measures of statistical significance and, even not explicitly stated, partial unloading in order to account for possible non-linearities in the specimen compliance.

A third expression to calculate the G_I value is called Modified Compliance Calibration method (MCC). From the beam theory modified in order to account for large rotation during loading, the following expression can be derived:

$$G_{Ic} = \frac{3}{2}\frac{P^2 C^{2/3}}{A_1 bh} \tag{8}$$

Here, the coefficient A_1 is determined as the intersection of the best fitting line of the experimental data given in terms of $C^{1/3}$ versus a/h with the vertical axis.
However, the G values estimated with Eqn (1), (6), have to be corrected again in order to account for the large displacement and the progressive reduction of the bending arm due to rotation around the hinge. In this case, the rotation to be applied is given as:

$$G_I = F \cdot G_I^0 \tag{9}$$

where G_I^0 is the value obtained with one of the relationships given above and F is the correction factor defined as

$$F = 1 - \frac{3}{10}\left(\frac{\delta}{a}\right)^2 - \frac{3}{2}\left(\frac{\delta t}{a^2}\right) \tag{10}$$

where t is the distance from the delamination crack mid-plane and the rotation center of the hinge.
Finally, a fourth method for the estimation of G is given by the evaluation of the area below the curve applied load and opening displacement measure for two crack lengths. In Fig. 2 the two limit cases, relative to the imposed load and displacement condition, are given.

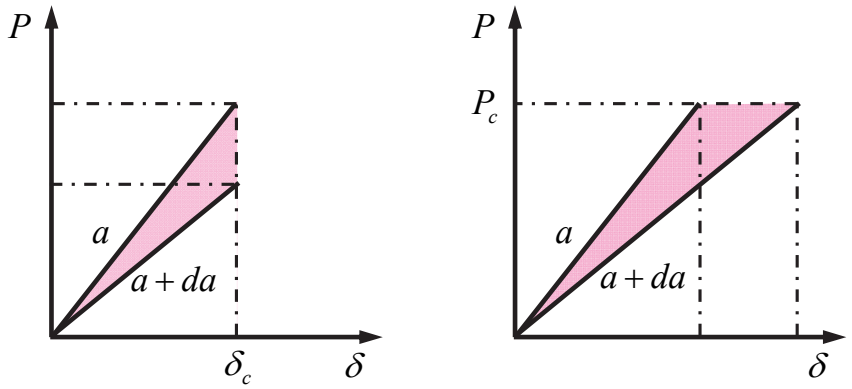

Figure 2: Theoretical definition of the strain energy release rate for a crack advance equal to *da*.

Even though this approach is not described in the prescription is a valuable and effective method for evaluating G in those cases where only few data points can be measured from a test. Since this method is based on the theoretical definition of G and does not requires the knowledge of other constants of material properties, is not limited by any assumptions and allows one to compensate the effect of eventual non-linearities in the load-displacement response of the specimen as well as the influence of the compliance of the measurement chain. According to this, it is suggested that, when possible, even though the ASTM D5528 prescriptions indicates to use alternatively one of the three methodologies (Modified Beam Theory, MBT, Compliance Calibration Method, CC, e Modified Compliance Calibration Method, MCC), a comparison with the values obtained with the area below the curve is also performed.
The experimental data measured on the DCB tests performed are detailed reported in the following section. For each sample, the measured load, applied displacement and crack advance are given and the G values are calculated with three procedures indicated above, when enough data are available. Samples showing geometrical oddness or where extensive fiber bridging was observed are highlighted and eventually excluded from statistical considerations.

Preliminary considerations and fundamental relationships for laminate fracture resistance under mode II

The same notched beam geometry configuration used for the DCB can be used in order to load the crack under pure mode II (sliding). In this case, the sample is loaded in three points bending conditions.

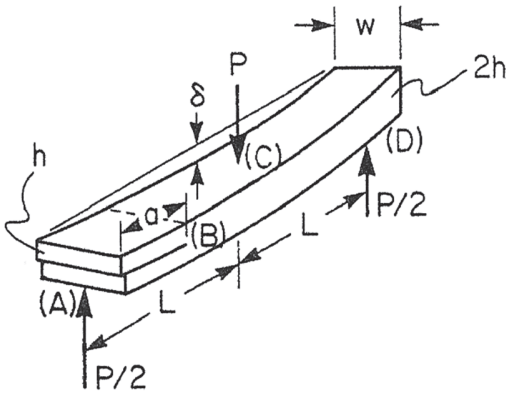

Figure 3: ENF geometry configuration and dimensions

This configuration has been found to produce shear loading at the crack tip without introducing excessive friction between the crack surfaces, [10, 11].
From the classical beam theory, the following expression for the GII can be derived, [12]:

$$G_{II} = \frac{9P^2Ca^2}{2w(2L^3 + 3a^3)} \tag{11}$$

where the specimen compliance C is given by:

$$C = \frac{2L^3 + 3a^3}{8E_{f1}wh^3} \tag{12}$$

The stability of the crack growth may be estimated by the sign of the first derivative with respect to the crack advance, ∂a. Eqn. (11) and (12) for fixed load lead to:

$$\frac{\partial G_{II}}{\partial a} = \frac{9aP^2}{8E_{f1}w^2h^3} \tag{13}$$

while for fixed displacements,

$$\frac{\partial G_{II}}{\partial a} = \frac{9a}{8E_{f1}w^2h^3}\frac{\delta}{C^2}\left[1 - \frac{9a^2}{2L^3 + 3a^3}\right] \tag{14}$$

The first condition is always defined positive indicating that this configuration is always unstable. On the contrary the second condition is negative (i.e. stable crack growth) only for

$$a \geq \frac{L}{\sqrt[3]{3}} \simeq 0.7L \tag{15}$$

Since in most of the cases a is usually close to L/2, this configuration always leads to unstable crack growth. Consequently, very few experimental data points (theoretically just one) are expected to be measured on a single sample.
The estimation of the fracture toughness requires a record of the load displacement response. In the case of ductile matrix where nonlinearities in the load vs displacement curve may occur, the G_{II} at the onset non-linearity, visual stable crack extension and maximum load can be determined as illustrated schematically in Fig. 4a.

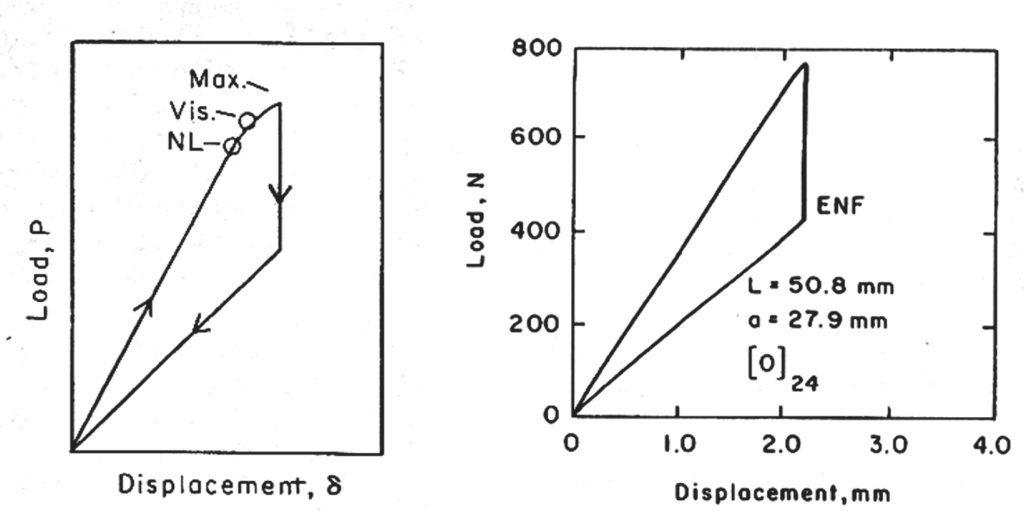

a) b)

Figure 4: Examples of ENF responses for ductile and brittle matrix.

Thus, the fracture toughness is calculated from the following beam theory expression:

$$G_{IIc} = \frac{9a^2P^2\left(C - C_{SH}\right)}{4wL^3\left[1+1.5\left(a/L\right)^3\right]} \tag{16}$$

where

$$C_{SH} = \frac{6L + 3a - L^3/a^2}{20whG_{13}} \tag{17}$$

In the EN6034 prescription the nomenclature is slightly different and in particular the entire span is L*=2L. Consequently, Eqn. (11) becomes:

$$G_{II} = \frac{9P\delta a^2}{2w(0.25L^{*3} + 3a^3)} \tag{18}$$

EXPERIMENTAL TECHNIQUE

A quasi-static electro-mechanical traction machine GALDABINI SUN10/P has been used for the testing. During each test, both the crosshead displacement and the applied load have been recorded. Preliminary system calibration has also been performed particularly to check the behavior of the two hinges used in the DCB test configuration and the bonding technique used to apply them to the specimens.
The material investigated is a carbon fiber/epoxy unidirectional laminate with different configurations in terms of resin volume and cure or fiber. Initially, DCB and ENF samples from different laminate types have been produced, examined, and identified according to the nomenclature given in Tab. 1.
Investigated materials are very close to commercial T1000 and M30 produced by TORAYCA®, at the moment is not allowed to the author to give further indications.
A total of 61 tests have been performed.

DCB hinges selection and assessment

As far as concerns the DCB configuration tests, load has been applied by means of two hinges as suggested in the ASTM prescriptions, Fig. 5, [13].

Material	Thickness [mm]	DCB available	DCB tested	DCB rejected	ENF available	ENF tested	ENF rejected
TA1	3.8	6	6	0	6	0	6
T3	5.0	6	6	0	6	4	0
T6	5.0	5	3	2	5	4	0
M1	7.3	5	5	0	5	0	0
M8	7.3	7	7	0	7	4	0
L1	3.8	9	9	0	9	4	0
L2	3.8	9	5	0	9	4	0
Total		47	41	2	47	20	6

Table 1: Summary of materials and specimens available and tested.

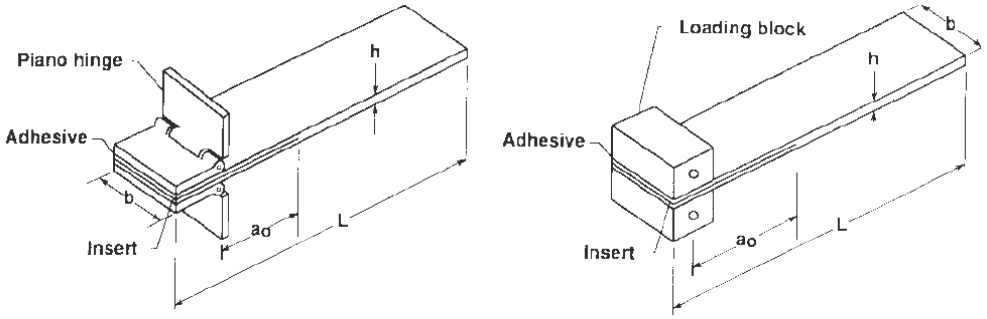

Figure 5: Sketch of the possible loading configuration using hinges or loading block in DCB specimen, ASTM : D 5528, [13].

The hinge selection has been made based on the estimated maximum load expected in test as given by:

$$P_{\max} = \frac{b}{a}\sqrt{\frac{h^3 E_{11} G_{Ic}}{96}} \tag{19}$$

Assuming
$E_{11} = 150\ GPa$
and conservatively
$G_{Ic} = 1.5\ kJ/m^2$, $h = 4\ mm$, $b = 25\ mm$, with $a = 50\ mm$
the maximum expected load found is 193 N, that is 20 kg approximately. Based on this estimation, a steel plane hinge available on-the-shelf, W=25, L=50 and t=1.0 mm long, has been selected
The length of the hinge wing bonded to the specimen has been reduced to 25 mm. The other hinge wing (50 mm) allows a proper grip and positioning with the testing machine gripping fixture, as shown in Fig. 6.
In order to avoid that the hinge could eventually loose under the applied load resulting in an increase of the overall compliance, a traction test has been performed in order to measure the maximum allowable load in tension. This value resulted to be 1200 N approximately, much higher of the maximum load expected for the used experimental configuration.
The perfect adhesion between the specimen external surface and the hinge wing is fundamental for the good result of the test. A poor adhesion may result in a partial debonding and, consequently, in an apparent increase of the specimen compliance and error in the G_I estimation. In order to identify the best configuration three different epoxy bi-component glues have been tested. It is important to underline that a brittle glue would eventually result in a premature detachment of the hinge while a too ductile glue would result in an excessive deformation and incomplete load transfer. In all the cases the

performances were comparable and in the acceptance range. The nominal normal separation stress for the tested glues was 160 Kg/cm² approximately. Based on the experimentalist confidence, the best performances have been obtained with a bi-component glue from PATTEX. The glue hardening time is 15 min. approximately but the full load carrying capabilities are obtained after 24h curing time at room temperature. The sample external surface has been previously polished using sand paper in order to increase the surface roughness for an optimal bonding without damaging the material. For each sample the planarity of the hinge wings has been checked before bonding. In order to ensure a uniform glue layer thickness and to avoid relative sliding during curing, a uniform pressure has been applied by means of calibrated weights. This procedure resulted in a two stages gluing for both plane hinge wings carefully avoiding positioning errors.

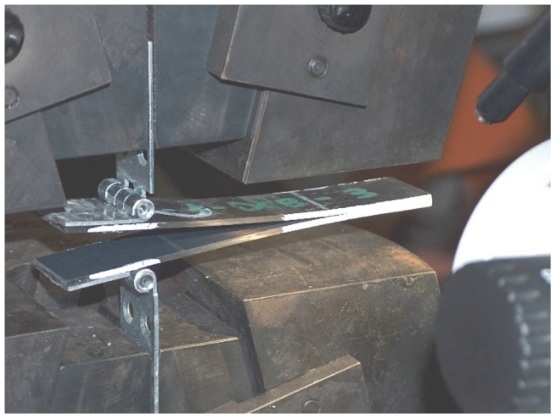

Figure 6: Detail of the gripping fixture showing the different length of the hinge wings.

Specimen preparation

In order to perform the measure of the crack extension during the delamination process it is necessary to draw a scale along the expected crack path. The fact that the material under investigation is made of carbon fiber makes very difficult to visualize the current crack length and to trace visible markers. The sample thickness has been initially covered with water-based liquid paper. Successively a graduated ruler with a minimum step of 1.0 mm has been traced along the crack path. This operation has been performed paying maximum attention in order to minimize possible errors verifying the measure with a caliper at different locations. In Fig. 7, a detail of a prepared sample is given for reference.

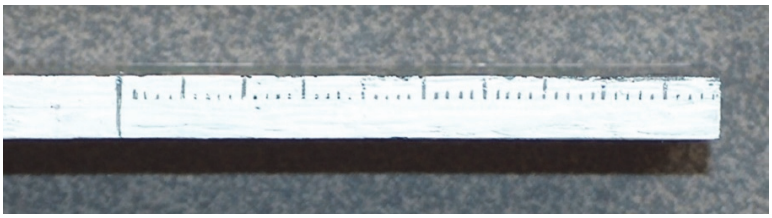

Figure 7: Detail of the length scale for crack advance measurements, step: 1mm.

Three point bend apparatus

ENF test requires appropriate three points bend fixture to be performed. For the present investigation, an adaptable span fixture has been built on purpose. Particular attention has been paid to the dimensions and mass of the fixture in order to avoid any possible influence on the measure of the G_{II} of the fixture compliance. The fixture, depicted in Fig. 8, has been realized according to the ASTM standard.

EXPERIMENTAL RESULTS

DCB specimens

The specimen has been grouped according to the type of the ply. For each test has been recorded the applied load vs imposed displacement. The measured crack advance as a function of the imposed displacement is also collected. These values are used to calculate the corresponding G values. If more than three data point are available, the G

has been calculated with the three methods previously discussed and a crack resistance curve has been recorded. In some cases, only a single estimation of G was possible due to problems in the propagation such as extensive fiber bridging and loss of planarity of the running crack.

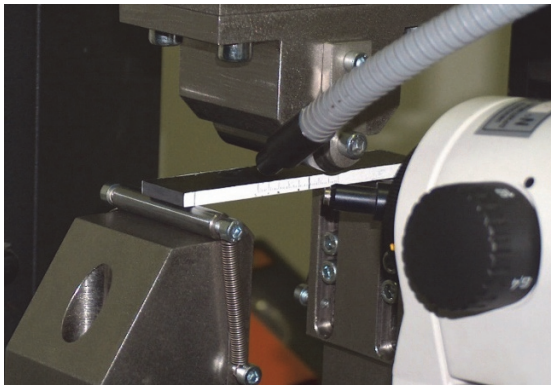

Figure 8: Detail of the three point bending fixture for ENF mode II tests.

The experimental results relative to DCB tests have been analyzed in order to derive statistical trends. Firstly, the data have been analyzed grouping all the crack resistance measurements by specimen sets, which is by different lamina type. Successively, the same data have been grouped based on the thickness of the samples independently on the material. Only the samples for which more than three crack advance data points have been collected are considered in the following analysis. The G values are those obtained with the compliance calibration method (CC). Since the occurrence of fiber bridging phenomenon characterizes crack propagation in most of the tested samples, all the data points have been considered in the following statistics since it is opinion of the author that this may contribute in evaluating the effective material data scatter expected.
For each graph, the following quantities are given in the summary table:
A: Intercept value and its standard error.
B: Slope value and its standard error.
R: Correlation coefficient.
P: value - Probability (that R is zero).
N: Number of data points.
SD: Standard deviation of the fit
In Fig. 9 e in Tab. 2 are reported the results for material designed TA1.

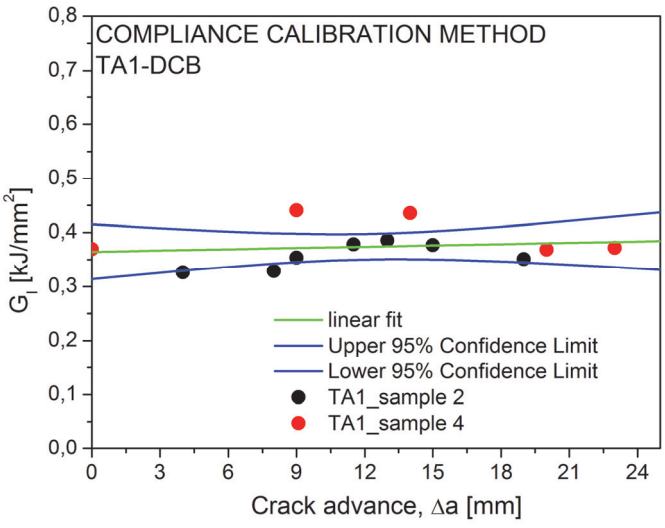

Figure 9: TA-1 Summary of crack resistance data.

Parameter	Value	Error	
A	0.3642435	0.0227864	
B	7.9023084E-4	0.0016625	
R	SD	N	P
0.1486407	0.0368036	12	0.6447683

Table 2: Linear regression for TA-1: $y = A + Bx$

In Fig. 10 and in Tab. 3 are reported the results for material designed L2.

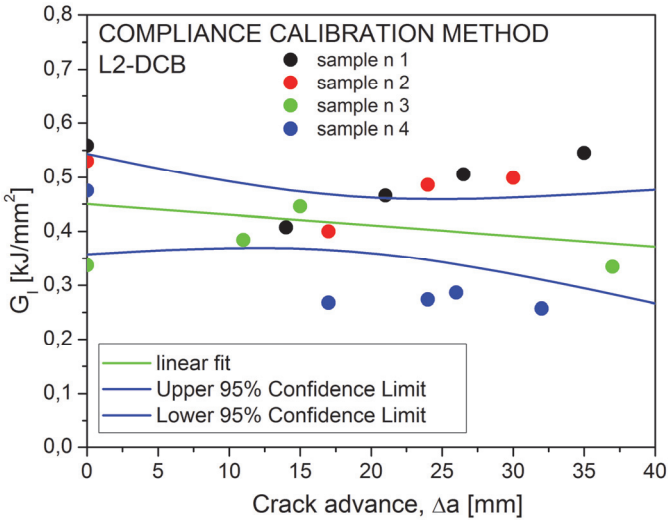

Figure 10: L2 Summary of crack resistance data.

Parameter	Value	Error	
A	0.4503601	0.0437614	
B	-0.0019675	0.002001	
R	SD	N	P
-0.2387065	0.1015897	18	0.3401201

Table 3: Linear regression for L2: $y = A + Bx$

In Fig. 11 e in Tab. 4 are reported the results for material designed L1.

Parameter	Value	Error	
A	0.2498155	0.0282799	
B	-3.5147405E-4	0.00176	
R	SD	N	P
-0.0889539	0.0444284	7	0.8495839

Table 4: Linear regression for L1: $y = A + Bx$

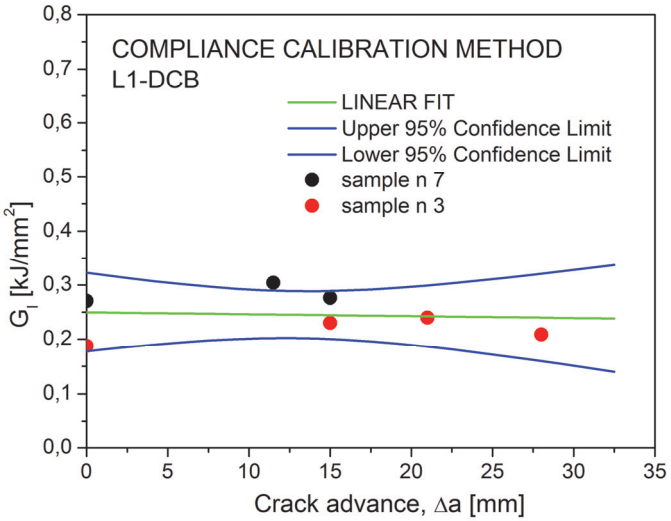

Figure 11: L1 Summary of crack resistance data.

In Fig. 12 and in Tab. 5 are reported the results for material designed T-1000-3.

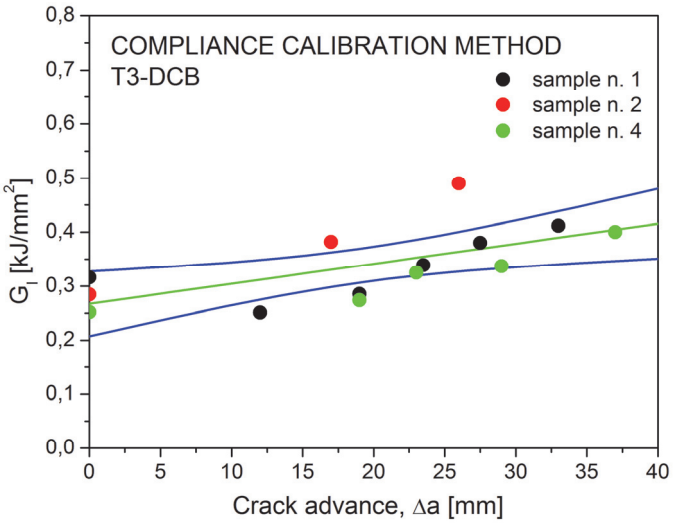

Figure 12: T3 Summary of crack resistance data.

Parameter	Value	Error		
A	0.267281	0.02757		
B	0.0037055	0.00124		
R		SD	N	P
0.65439		0.05407	14	0.0111

Table 5: Linear regression for T3: $y = A + Bx$

In Fig. 13 and in Tab. 6 are reported the results for material designed T6.

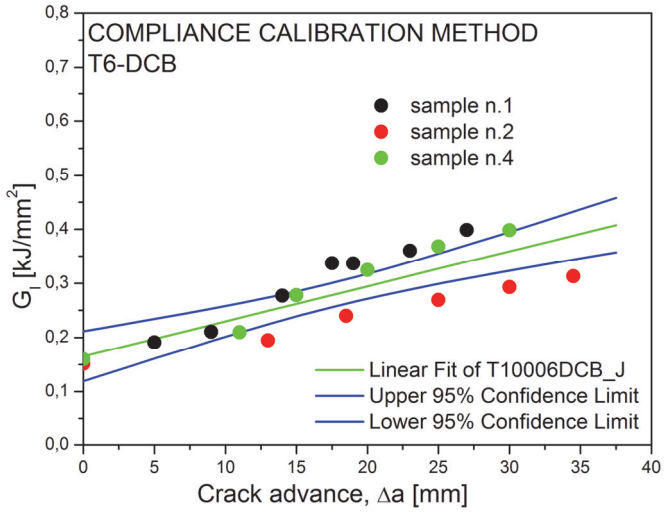

Figure 13: T6 Summary of crack resistance data.

Parameter	Value	Error	
A	0.1651137	0.0219622	
B	0.0064593	0.0010892	
R	SD	N	P
0.8210532	0.0457617	19	0.0001

Table 6: Linear regression for T6: $y = A + Bx$

In Fig. 14 and in Tab. 6 are reported the results for material designed M30-1.

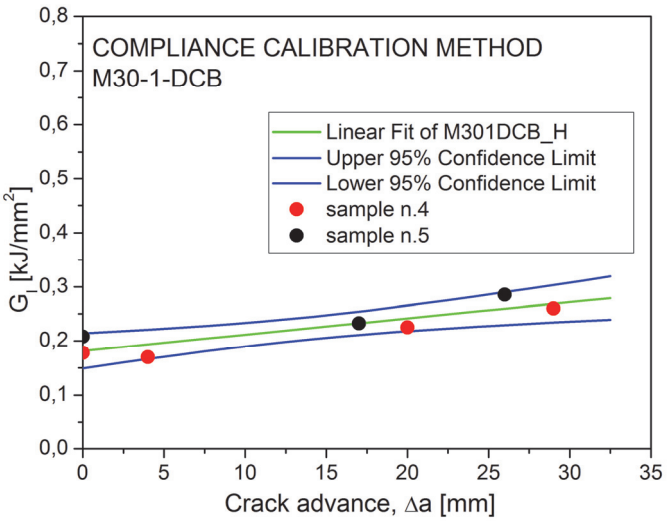

Figure 14: M30-1 Summary of crack resistance data.

Parameter	Value	Error	
A	0.1814411	0.0126216	
B	0.0030053	7.08419E-4	
R	SD	N	P
0.8846366	0.0213166	7	0.0081516

Table 7: Linear regression for M30-1: $y = A + Bx$

In Fig. 15 and in Tab. 8 are reported the results for material designed M30-8

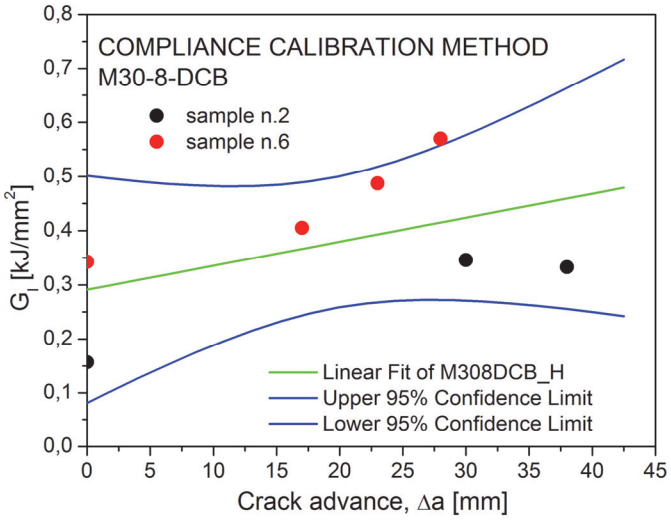

Figure 15: M30-8 Summary of crack resistance data.

Parameter	Value	Error	
A	0.2910397	0.081719	
B	0.0044296	0.0034419	
R	SD	N	P
0.4988296	0.1242753	7	0.2544621

Table 8: Linear regression for M30-8: $y = A + Bx$

A summary of strain energy release rates for DCB tested materials is reported in Fig. 16.
A summary of strain energy release rates for DCB tested specimens vs. thickness is reported in Fig. 17. There is no distinction about materials but only different thickness of the samples.
In Fig. 18 is reported a sample of bridging fibers in DCB specimens.

ENF specimens

In the following, similarly to the DCB results, the ENF data, for each specimen tested, are given. For what concerning G_{II}, in addition to the value calculated with the relationship given in the prescription EN6034, other two values, the nonlinear and visual nonlinear, are also given, Fig. 4a. As discussed in the previous paragraph, the crack propagation resulted to be unstable for all specimens tested and only a single value of G_{II} could be determined since, after the propagation, the crack extends up to the specimen midspan L where no further propagation is possible.
The results are summarized in Tab. 9.

Fig. 19 shows the G_{II} values (max min and average) calculated at maximum load. It is possible to note that the material L1 and T1000-3 give a shorter dispersion data. For these materials bridging occurs less time that the others materials.

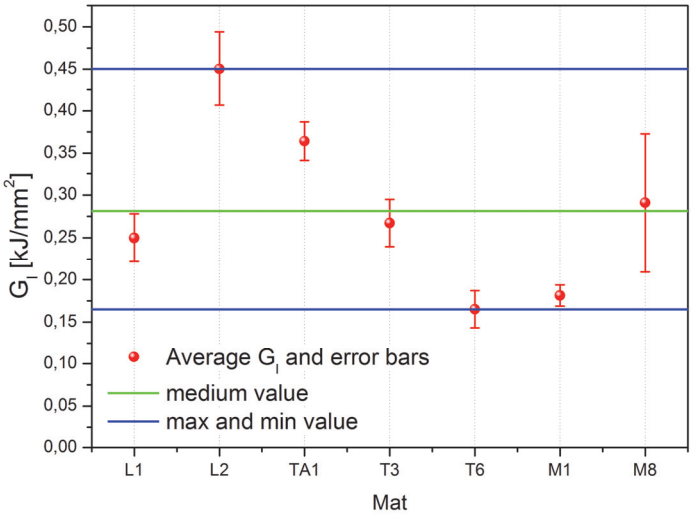

Figure 16. Summary of strain energy release rates for tested materials.

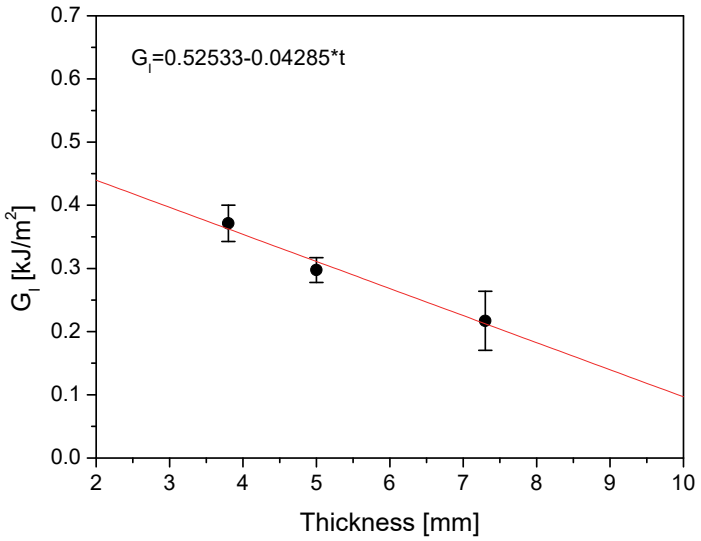

Figure 17. Average strain energy release vs specimen thickness.

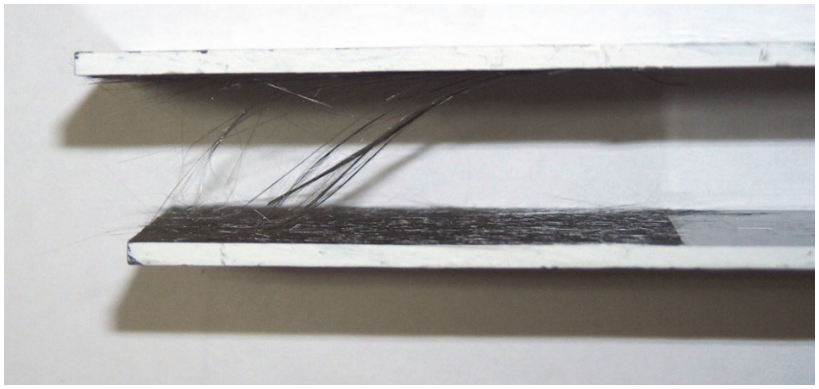

Figure 18. Bridging in a DCB specimen.

Average G_{II} [KJ/m²]			
MAT	NL	VIS	MAX
L1	1.05566	1.18446	1.19325
L2	1.3823	1.41844	1.42526
T3	1.55113	1.65783	1.66877
T6	0.98038	1.06658	1.08361
M30_8	1.47872	1.56995	1.58716

Table 9: Average GII values from ENF tests (NL=non-linearity; VIS= visual stable crack extension; MAX= maximum load, see Fig. 4a).

An example of average G_{II} calculation is given in Fig. 19 for Material T3.

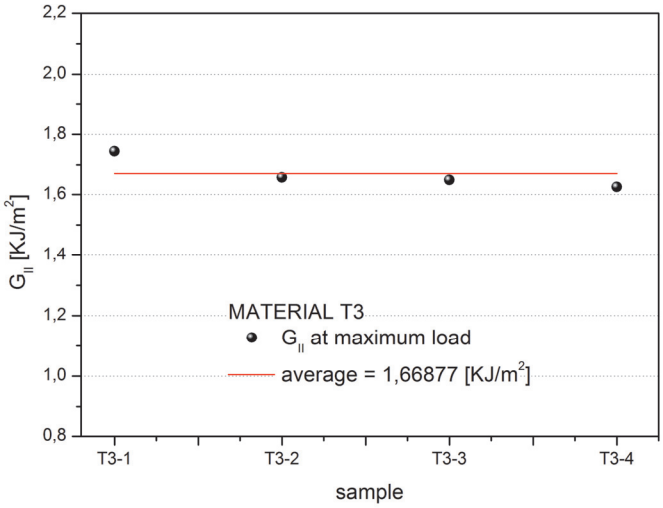

Figure 19: G_{II} at max load for material T3.

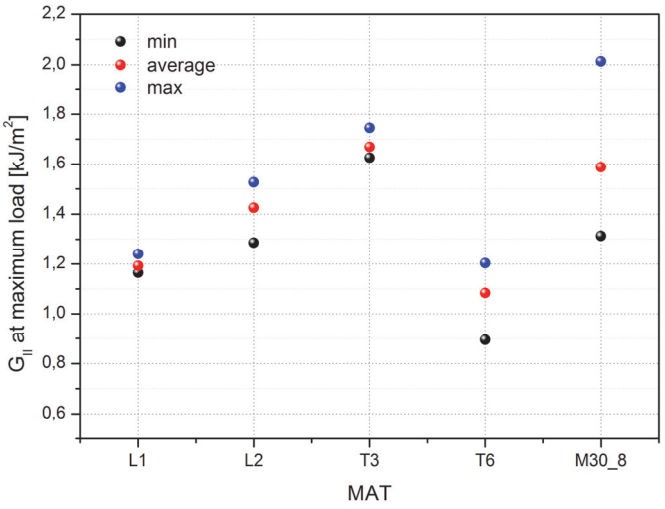

Figure 20: G_{II} calculated at maximum load.

CONCLUSION

In this preliminary work, delamination mode I and mode II was investigated for different composites made of carbon fiber and epoxy matrix.
Test results will be used in order to define a correct experimental procedure for further investigations and as data information for Finite element analysis that will be performed in order to simulate the behavior of a real aircraft component under loading conditions.
Bridging (Fig. 18) affected test results. Although bridging improve the material's delamination resistance, the more common was the bridging, the higher was the experimental scatter.
The material design T6 and M1 will be excluded for further consideration because have the lowest critical values of G_I and G_{II}.
Material M8 will be excluded also because bridging problems have given a high experimental scatter.
The materials candidate to further investigations seem to be L2 and T3.
L2 shows the highest values of G_I and a higher value of G_{II} but shows also bridging problems.
T3 has a higher G_I and G_{II} values and reduced experimental scatter respect to the others materials investigated as showed in Fig. 19.

REFERENCES

[1] Wilkins, D.J., Eisenmann, J.R., Camin, R.A., Margolis, W.S., Benson, R.A., Characterizing delamination growth in graphite–epoxy, damage in composite materials, ASTM Special Technical Publication, 775 (1980) 168–83.
[2] Whitney, J.M., Browning, C.E., Hoogsteden, W., A double cantilever beam test for characterizing mode I delamination of composite materials, Journal of Reinforced Plastics and Composites, 1 (1982) 297-313.
[3] Ratwani, M.M., Deo, R.B., Resistance curve approach to composite materials characterization, fracture mechanics. ASTM Special Technical Publication, 905(17) (1986) 108–123.
[4] Wang, Q.Z., A sandwich three-point bend specimen for testing mode-I interlaminar fracture toughness for fiber-reinforced composite materials, International Journal of Fracture, 85 (1997) 231–240
[5] Miyagawa, H., Sato, C., Ikegami, K., Interlaminar fracture toughness of CFRP in Mode I and Mode II determined by Raman spectroscopy. Composites: Part A, 32 (2001) 477–486.
[6] Svensson, D., Alfredsson, K.S., Biel, A., Stigh, U. Measurement of cohesive laws for interlaminar failure of CFRP. Composites Science and Technology, 100(21) (2014) 53–62. DOI: 10.1016/j.compscitech.2014.05.031.
[7] Pipes, R.B., Pagano, N.J., Interlaminar stresses in composite laminates under uniform axial extension, J. Comp. Mat., 4 (1970) 538-548.
[8] Wang, S.S., Fracture mechanics for delamination problems in composite materials, J. Comp. Mat., 17 (1983) 210-223.
[9] AECMA PREN 6034-1995, Aerospace Series Carbon Fibre Reinforced Plastics Test Method Determination of Interlaminar Fracture Toughness Energy Mode II - GIIc Edition P1, (1995).
[10] Carlsson, L.A., Gillespie, J.W., Pipes, R.B., On the analysis and design of the End Notched Flexure (ENF) specimen for mode II testing, J. Comp. Mat., 20 (1986) 594-604.
[11] Gillespie, J.W., Carlsson, L.A., Pipes, R.B., Finite element analysis of the end notched flexure specimen for measuring mode II fracture toughness, Compos. Sci. and Tech., 26 (1986) 177-197.
[12] Russel, A.J., and Street, K.N., 1985, Moisture and temperature effects on mixed mode delamination fracture of unidirectional graphite/epoxy, ASTM STP 876, (1985) 349-370.
[13] ASTM standards D 5528 – 01 (Reapproved 2007).